

Supported lipid bilayer/carbon nanotube hybrids

XINJIAN ZHOU^{1*}, JOSE M. MORAN-MIRABAL², HAROLD G. CRAIGHEAD² AND PAUL L. McEUEN^{1*}

¹Laboratory of Atomic and Solid-State Physics, Cornell University, Ithaca, New York 14853, USA

²Applied and Engineering Physics, Cornell University, Ithaca, New York 14853, USA

*e-mail: xz58@cornell.edu; mceuen@ccmr.cornell.edu

Published online: 25 February 2007; doi:10.1038/nnano.2007.34

Carbon nanotube transistors combine molecular-scale dimensions with excellent electronic properties, offering unique opportunities for chemical and biological sensing. Here, we form supported lipid bilayers over single-walled carbon nanotube transistors. We first study the physical properties of the nanotube/supported lipid bilayer structure using fluorescence techniques. Whereas lipid molecules can diffuse freely across the nanotube, a membrane-bound protein (tetanus toxin) sees the nanotube as a barrier. Moreover, the size of the barrier depends on the diameter of the nanotube—with larger nanotubes presenting bigger obstacles to diffusion. We then demonstrate detection of protein binding (streptavidin) to the supported lipid bilayer using the nanotube transistor as a charge sensor. This system can be used as a platform to examine the interactions of single molecules with carbon nanotubes and has many potential applications for the study of molecular recognition and other biological processes occurring at cell membranes.

Single-walled carbon nanotubes (SWNTs)¹ offer unique opportunities for chemical² and biological sensing^{3,4}. SWNT transistors⁵ have mobilities⁶ that exceed those of silicon and have transverse dimensions comparable to a strand of DNA. They also work efficiently in aqueous environments⁷ and, unlike silicon-based biosensors, they do not require an insulating layer to separate the ions from the conducting channel. An exciting possibility is to use a nanotube to probe the properties of lipid membranes and their functional constituents. Supported lipid bilayers (SLBs)^{8–10} self-assemble from phospholipids on flat hydrophilic substrates like glass and mimic many properties of cell membranes. The lipids in an SLB are laterally mobile, and many reconstituted membrane proteins embedded in them remain functional^{11,12}. Although it has been shown that lipid bilayers can form on top of multiwalled carbon nanotubes¹³ or SWNTs coated with polyelectrolytes¹⁴, the nanotubes in these experiments were not used as detection elements and the bilayers were not supported on flat substrates. Another group has placed membrane patches on SWNT field-effect transistors (FETs)¹⁵, but no continuous SLBs were formed and the measurements were carried out in dry conditions.

Here, we show the integration of SLBs with SWNT FETs (Fig. 1). We first demonstrate membrane continuity and lipid diffusion over the tube. However, we also show that the nanotube acts as a diffusion barrier for a membrane-bound tetanus toxin protein, and that the strength of the barrier depends on the diameter of the nanotube. Finally, we present results on the electrical detection of specific binding of streptavidin to biotinylated lipids. The formation of fluidic SLBs on SWNTs will allow the study of lipid–SWNT interactions and sensing of analytes binding to specific receptors embedded in the SLBs. These studies should have an impact on our understanding of model and biological membranes.

PHYSICAL PROPERTIES OF SLB/SWNT HYBRID STRUCTURES

We first formed 1,2-dioleoyl-sn-glycero-3-phosphocholine (DOPC) SLBs on chips containing SWNTs (see Methods). Before examining the regions around the nanotubes, we tested the overall quality of the SLBs on SiO₂ using two criteria. First, SLBs should be spatially uniform, as measured by fluorescence microscopy. Second, the lipid molecules in SLBs should be laterally mobile, as observed using fluorescence recovery after photobleaching (FRAP)¹⁶. For this, the fluorophores inside a region are bleached with long exposure to light and, once the bleaching is finished, the fluorescence in this region is allowed to recover by diffusion. The diffusion coefficients can be measured using FRAP or fluorescence correlation spectroscopy (FCS)¹⁷ (see Sections I and II of Supplementary Information). Both methods rely on the lateral diffusion of fluorescent lipids into a probed volume, which only occurs if the bilayer is continuous and laterally fluid. The diffusion coefficients, D , for the DOPC bilayers were extracted from fits to the FCS autocorrelation curves (see Methods), giving a value of $D = 5.4 \pm 0.1 \times 10^{-8} \text{ cm}^2 \text{ s}^{-1}$. This value compares favourably with previously published values¹⁸. With proper surface preparation, both criteria can routinely be met.

To test the continuity and fluidity of the formed SLB over a nanotube, we used FRAP on devices with the geometry shown in Fig. 2a. We created two square SLB patches¹⁹ connected by a 2- μm -wide, 12- μm -long channel. Nanotubes emerging from the black catalyst islands (visible in the optical micrograph) cross the channel. We photobleached the fluorophores in the right square and observed whether the fluorescence could recover by the diffusion of fluorophores from the left box across the nanotube to the right box. Figure 2b–d shows fluorescence images of the recovery process. It may be observed that fluorescent lipids can diffuse across the nanotube. No discernible

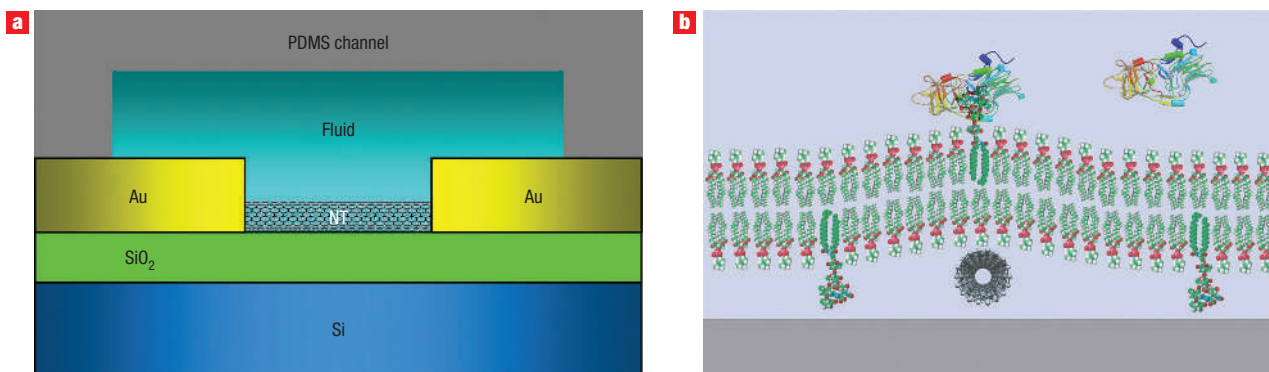


Figure 1 Representation of the SLB/carbon nanotube (NT) hybrids. **a**, Schematic of the side view of a SWNT FET inside a PDMS microfluidic channel. **b**, Scaled schematic of a carbon nanotube under a DOPC bilayer. The DOPC lipid molecules are shown with two light green fatty acid chains. A toxin protein, represented in a ribbon model, binds to a membrane-embedded ganglioside molecule that is shown with two dark green chains. There is a thin water layer between the SLB and the substrate.

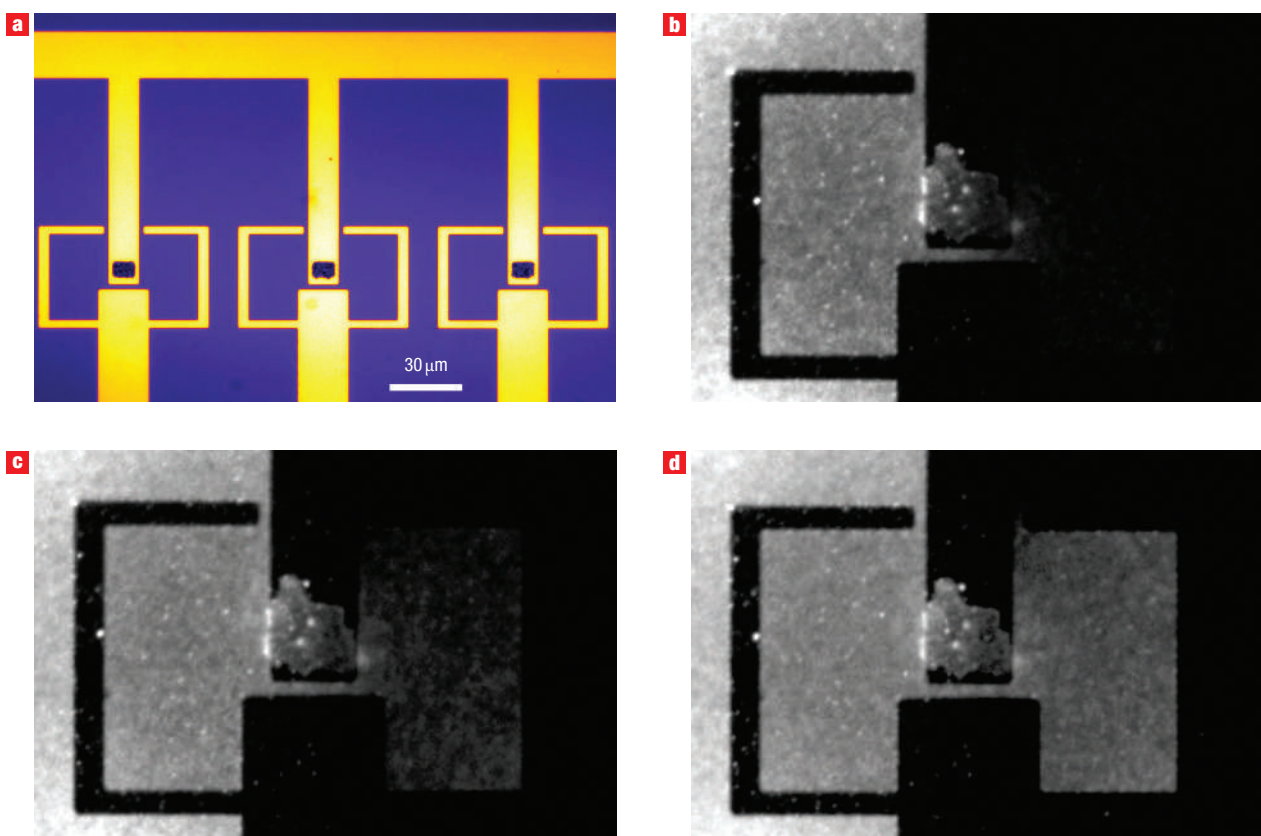


Figure 2 Test of lipid diffusion near SWNTs. **a**, Optical micrograph of SWNT FET array used for diffusion tests. Two isolated regions of SLB are defined by gold electrodes and connected by a narrow channel crossed by nanotubes. **b–d**, Fluorescence images taken 2.5 min (**c**) and 10 min (**d**) after fluorophores on the right side were originally bleached (**b**). The lipids diffuse freely across the nanotube.

differences were observed between the FRAP recovery over a nanotube and control experiments with the same geometry but without nanotubes. A second experiment was performed to confirm that the lower leaflet of the SLB was also continuous. In this experiment, 100 mM CoCl_2 was added to the buffer solution in the channel to quench the fluorescence coming from the

fluorophores on the upper membrane leaflet²⁰. The FRAP experiment described above was then repeated to probe the fluorescence recovery of the lower leaflet only. The recovery speed remained the same, within a 10% error. These experiments show that lipid bilayers are continuous and that lipids freely diffuse over nanotubes.

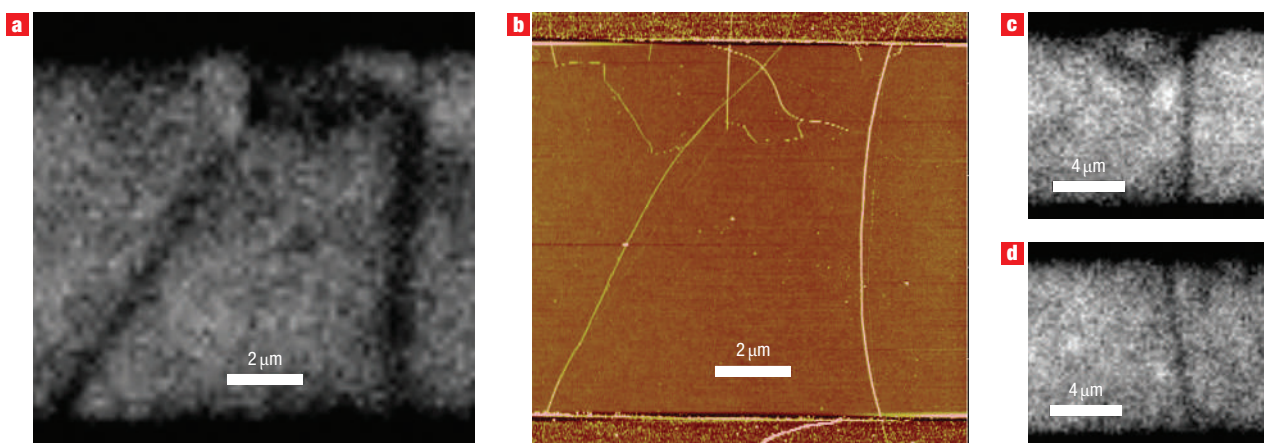


Figure 3 Fluorescence intensity distribution around the SWNTs. **a**, Fluorescence image of the gap region between the electrodes of a SWNT FET. Several dark linear features were observed. **b**, AFM image of the region in **a** after the SLB was removed. It is clear that the dark lines in **a** correspond to the position of the nanotubes. **c,d**, Two more fluorescence images of SWNTs showing up as dark lines.

A surprising result was seen when we examined the SLB fluorescence in the vicinity of the nanotubes. Linear features corresponding to a slight reduction ($\sim 2\text{--}7\%$) in the fluorescence intensity were observed, as shown in Fig. 3a. Figure 3b is an atomic force microscope (AFM) image showing the same region as that displayed in Fig. 3a. It is evident that the dark lines in the fluorescence image correspond to the positions of the carbon nanotubes. The results were unaffected by a polarizer added parallel or perpendicular to the axis of the nanotubes. For the eight tubes studied, there was no obvious correlation between the tube diameter and the magnitude of the suppression. The width of the fluorescence suppression features is approximately $0.5\ \mu\text{m}$, set by the resolution of the imaging system. If we use the simplest possible scenario and assume that the fluorophores closest to the nanotube are completely dark, the observed reduction in fluorescence would correspond to a band approximately $10\text{--}35\ \text{nm}$ wide.

The observed fluorescence suppression at the nanotubes could be a result of many factors. An obvious explanation is that the SLB is interrupted by the nanotube, but this possibility is ruled out by the FRAP experiments described above. Another possibility is that the nanotubes quench the fluorescence of any fluorophores in their vicinity. We expect the range of quenching to be approximately $d + 2R_0$, where d is the diameter of the nanotube and R_0 is the Förster radius²¹. Although R_0 is unknown here, typical values are $\sim 5\ \text{nm}$, which predicts a quenched width of $\sim 10\text{--}15\ \text{nm}$. This is in reasonable agreement with the magnitude of the measured signal. Another possibility is that the local curvature induced in the SLB by a nanotube excludes the fluorescently labelled lipids. Such curvature-induced segregation of lipid species has been seen in previous experiments^{22–24}.

NANOTUBES AS BARRIERS TO PROTEIN DIFFUSION

Having established that the SLB is continuous over the nanotube, we now examine the influence of the nanotube on SLB-bound macromolecules. To test the diffusion of membrane-bound proteins over the nanotubes, we chose a simple and well-studied toxin–ganglioside couple^{25,26} as the model system (Fig. 1b). Tetanus and cholera toxins are part of a family of bacterial toxins that bind to glycolipid moieties present on the host cell's membrane as a path

for infection. Tetanus toxin fragment C (TTC) binds to tri sialoganglioside G_{T1b} , and cholera toxin subunit B (CTB) binds strongly to mono sialoganglioside G_{M1} . The lipid mixtures used for toxin binding consisted of 99:1 DOPC/ G_{M1} -BODIPY (4,4-difluoro-5,7-dimethyl-4-bora-3a,4a-diaza-s-indacene) (Molecular Probes) for the cholera system, or 98.9:1:0.1 DOPC/ G_{T1b} /DHPE-LR (Lissamine-Rhodamine Red 1,2-dihexadecanoyl-sn-glycero-3-phosphoethanolamine) for the tetanus system. We first formed SLBs with these lipid mixtures on wafers containing nanotubes and performed FRAP studies of the ganglioside diffusion properties across the nanotubes before protein binding. Using the BODIPY fluorophore attached to G_{M1} , experiments analogous to those presented in Fig. 2 demonstrated that the gangliosides can diffuse across nanotubes with no measurable hindrance.

Strikingly different results were obtained after the gangliosides were incubated with toxin fragments using either G_{M1} -CTB or G_{T1b} -TTC systems. FRAP experiments on ganglioside-bound toxins showed marked diffusion hindrance across the nanotubes. To quantitatively measure this diffusion barrier, we used fluid flow to apply a lateral driving force to the ganglioside-bound toxins²⁷. The flow within the channel was generated by applying a pressure gradient across the channel, the maximum flow speed in the centre of the channel being measured at up to $1.5\ \text{mm s}^{-1}$. We used the G_{T1b} -TTC pair in which TTCs were labelled with Alexa 488 fluorophores. The flow created a hydrodynamic drag force and drove the toxin–ganglioside units in the direction of the flow. This drag force generated a gradient in the TTC profile, as shown in Fig. 4. In each of the three devices shown, the SLB is much brighter on the right side of the electrode than on the left, because the drag force drives the TTCs toward the left, where they build up against the electrode.

The most important features in Fig. 4 are in the channel connecting the left and right sides of the SLB. At the location where a nanotube crosses the channel, there is often a dramatic step in the fluorescence intensity profile. Figure 4d shows the TTC fluorescence intensity as a function of distance along the channel crossed by a 2.1-nm-diameter nanotube; the build-up of toxin upstream and the dramatic drop-off at the nanotube are clearly visible. AFM imaging verified that the discontinuity happened exactly where the nanotube crossed the channel. The upstream build-up and the sudden drop-off at the nanotube mean that the nanotube acts as a significant barrier to the

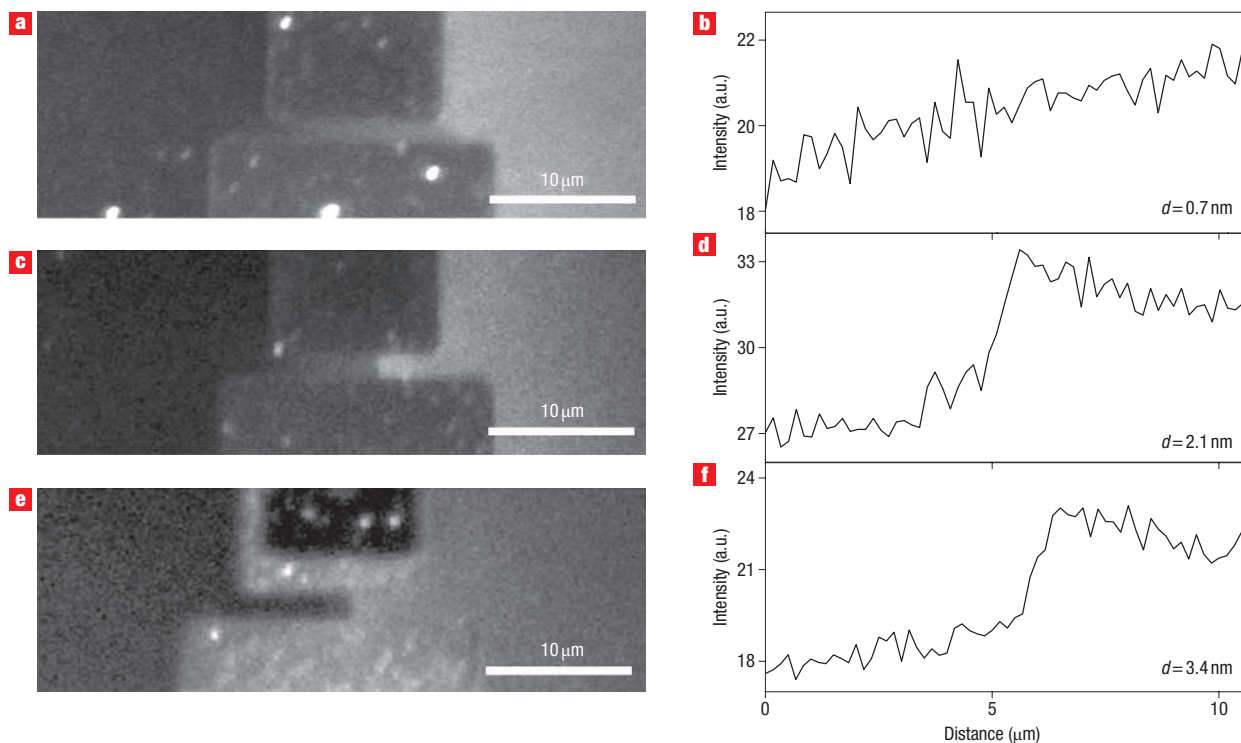


Figure 4 Driving ganglioside-bound toxins near SWNTs with flow. The fluid flow is driving the tetanus toxin towards the left side in all images. **a,c,e**, Fluorescence images of ganglioside-bound toxin distributions around SWNTs of 0.7 nm (**a**), 2.1 nm (**c**) and 3.4 nm (**e**) diameter. **b,d,f**, Fluorescence intensities along the gap for the SWNTs in **a**, **c** and **e**, respectively. The sharp steps in fluorescence intensity occur at the position of the nanotubes.

transport of the membrane-bound TTCs. Similar results are displayed for two other devices; the size of the barrier depends strongly on the nanotube diameter.

We can use the fluorescence intensity profiles to quantitatively determine the magnitude of the barrier presented by the nanotube to TTC transport. We first assume the fluorescence intensity is directly proportional to the toxin density, which is valid at low fluorophore concentration. We define n_L and n_R as the TTC density on the left and right side of the nanotube respectively, and $\Delta n = n_R - n_L$ as the sudden jump of TTC density at the nanotube. In the steady state, the flux density $J = \mu F n + D \frac{dn}{dx}$ should be equal on both sides of the nanotube. Here F is the hydrodynamic drag force on the toxin, and μ and D are the mobility and diffusion coefficient of the TTC, connected by the Einstein relation $D = \mu k_B T$. By considering the flux on both sides of the nanotube, we can deduce J :

$$J = \frac{D}{\Delta n} \left[\left. \frac{\partial n_L}{\partial x} \right|_{n_R} + \left. \frac{\partial n_R}{\partial x} \right|_{n_L} \right]$$

The permeability P of a barrier is defined as $J = P \Delta n$. Denoting $P_o = D/d$ as the permeability of a patch of lipid with width equal to the nanotube diameter, the ratio P/P_o is given by

$$\frac{P}{P_o} = \frac{d}{(\Delta n)^2} \left[\left. \frac{\partial n_L}{\partial x} \right|_{n_R} + \left. \frac{\partial n_R}{\partial x} \right|_{n_L} \right]$$

This normalized permeability represents the additional barrier caused by the nanotube and can be determined from the

fluorescence profile and the diameter of the nanotube. For the nanotube in Fig. 4c,d, $P/P_o \approx 1.2 \times 10^{-3}$. Normalized permeabilities for other tubes are shown in Table 1. We see that P/P_o is a sensitive function of tube diameter, with the barrier immeasurably small for $d < 1$ nm and immeasurably large for $d > 4$ nm. If we associate this reduction in permeability with thermal activation over a barrier using $P/P_o = \exp(U/k_B T)$, we obtain barrier heights of 0–8 $k_B T$ for nanotubes with diameters between 0.7 and 3.4 nm.

The suppression of lateral transport of membrane proteins by the nanotubes is reminiscent of similar behaviour in cellular membranes. Cells have a cortex²⁸, a network of linear proteins (for example, actin or spectrin²⁹) located adjacent to the plasma membrane, which provides structural support to the membrane and is involved in the dynamic remodelling of the plasma membrane^{30,31}. A hypothesis consistent with the appearance of functional microdomains is diffusion hindrance by the underlying protein scaffold. Thus, we believe that the diffusion hindrance induced by the nanotubes on membrane-bound proteins could be acting in the same way the protein scaffold works to restrict membrane protein diffusion between lipid microdomains.

Table 1 Summary of normalized permeabilities of four nanotube barriers.

	Device 1	Device 2	Device 3	Device 4
Diameter (nm)	3.4	2.1	1.8	0.7
P/P_o	5.1×10^{-4}	1.2×10^{-3}	5.6×10^{-3}	~ 1
$U(k_B T)$	7.6	6.7	5.2	~ 0

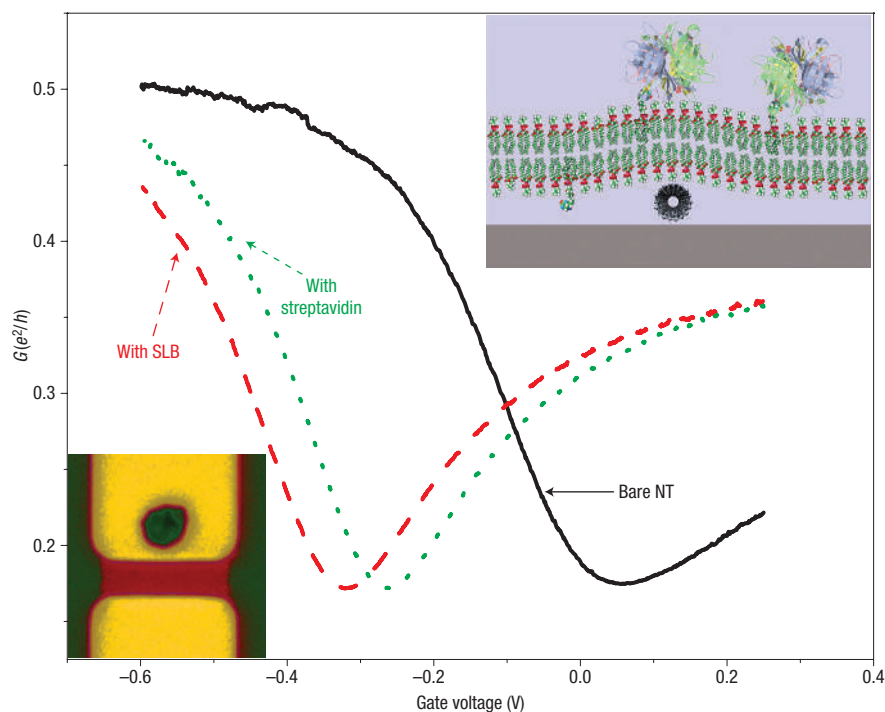


Figure 5 Detection of biotin–streptavidin binding with SWNT FETs. Conductance G versus electrolyte potential of a small-bandgap NT FET before (solid black) and after (dashed red) biotinylated SLB was formed on the surface. The dotted green curve was taken after streptavidin was bound to the membrane-embedded biotins. Lower inset: optical micrograph of devices used for sensing. The pink rectangular region between two yellow electrodes is the only opening in the Al_2O_3 insulation layer. Upper inset: schematic of a carbon nanotube under a biotin-functionalized lipid bilayer.

ELECTRICAL DETECTION OF PROTEIN BINDING

With the physical properties of SLB/SWNT hybrids established, we used the transistor properties of the nanotube to detect the specific binding of proteins to membrane-embedded targets. The streptavidin/biotin system³² was chosen for its high binding affinity. A mixed lipid composition, 93.9:4.2:0.1 DOPC/1,2-dioleoyl-3-trimethylammonium-propane(DOTAP)/1,2-dioleoyl-sn-glycero-3-phosphoethanolamine-N-(Cap Biotinyl)/DHPE-LR, was used to form SLBs functionalized with biotin, as shown in the upper-right inset of Fig. 5. It is worth noting that DOTAP has a positively charged headgroup (trimethylammonium group) whereas the biotinylated lipid contains a phosphoethanolamine which is negatively charged. To minimize ionic screening, 1 μM PBS buffer was used.

To isolate the electrodes from the electrolyte, the device was covered with a 30-nm-thick Al_2O_3 layer, except in the regions between the source and drain electrodes containing the nanotubes, as shown in the lower left inset of Fig. 5. The SLBs formed only in regions not covered with Al_2O_3 . Fluorescence microscopy revealed that the SLBs were uniform and laterally mobile, and that the streptavidin/biotin binding was stable, even after washing.

Figure 5 shows how the conduction of SWNT FETs was affected by SLB formation and streptavidin binding to the biotins imbedded in the SLBs (see Methods). The solid black curve in the main panel of Fig. 5 shows conductance G versus V_g before the lipids were added, and the red dashed curve was taken after the formation of SLB. The positively charged SLB significantly shifted the threshold voltage V_t of the nanotube FET. A shift was also observed when neutral SLBs formed on nanotube transistors (see Sections I and II of Supplementary Information), but the magnitude of the shift was larger with this positively charged

lipid mixture in low ionic strength buffer. The device was then incubated with 5 μM streptavidin for 10 min and rinsed. The bound streptavidin shifted V_t back towards positive voltages, as shown by the green dotted curve in Fig. 5. No shift was observed in control experiments with the addition of proteins that do not bind to biotin (for example, tetanus toxin), demonstrating the specificity of the detection.

For the six devices studied, the shift of threshold voltage ΔV_c caused by streptavidin binding was $\Delta V_c = 80 \pm 20$ mV. Using the model in ref. 33, which relates voltage shift induced by a layer of charge to its charge density, then $\sigma = 2\Delta V_c \epsilon_w \epsilon_0 / \lambda_d$, where ϵ_w is the dielectric constant of water and λ_d is the Debye length, and we estimate that the observed ΔV_c corresponds to an additional charge layer with $\sigma = -7 \times 10^3 e \mu\text{m}^{-2}$. The sign of σ agrees with streptavidins being negatively charged at the buffer pH, and the charge density is comparable to biotin density in the SLB of $3 \times 10^4 \mu\text{m}^{-2}$. The system studied is only one example of specific binding detection; any other charged protein that binds to a target located within the SLB should cause a similar effect on the SWNT FETs.

CONCLUSIONS

We have used electrical and fluorescence measurements to probe SLBs formed over carbon nanotube transistors. We show that the lipid molecules in a SLB can diffuse freely across nanotubes, but ganglioside-bound toxins see a nanotube-diameter-dependent diffusion barrier. We further demonstrate electrical detection of protein binding on the lipid bilayers with nanotube transistors. This new lipid/nanotube model system has many potential applications in the study of both electrical and mechanical perturbations at cell membranes. This system can also serve as a

generic platform for bringing mobile lipid-bound molecules and nanotubes into close proximity for studies of the physical, electrical and optical interaction of single molecules with nanotubes.

METHODS

FABRICATION OF NANOTUBE DEVICES

The SWNT FET devices (shown schematically in Fig. 1a) were fabricated as previously reported⁷. Carbon nanotubes were grown by chemical vapour deposition on silicon wafers with a 500-nm oxide capping layer. Using photolithography, gold electrodes were defined on top of the SWNTs with 2–10 μm gaps between source and drain electrodes. The nanotube growth yield was controlled so that most transistors had one nanotube bridging the electrodes.

DEVICE CLEANING

Wafers containing SWNT FETs were cleaned with room-temperature piranha solution (volume ratio 3:1 concentrated sulphuric acid/30% hydrogen peroxide) without sonication, or in a ultraviolet-ozone cleaner, to remove residual contamination from processing and render the surface hydrophilic. The cleaning procedures were developed to allow the formation of uniform fluid SLBs and were tested to ensure that they did not degrade the SWNT FET device performance. Most devices survive the cleaning procedures and their electrical conductance does not change by more than 20%.

FORMING AND IMAGING SLBS

The phospholipid used as a base for SLB formation was the zwitterionic 1,2-dioleoyl-sn-glycero-3-phosphocholine (DOPC, Avanti Polar Lipids). Small unilamellar vesicles (SUVs) were prepared as previously reported^{25,34}. Lipids were dissolved in chloroform at the appropriate molar ratios for a final concentration of 1 mM, and allowed to mix. The solvent was evaporated under a dry nitrogen stream, forming a uniform lipid film. The lipids were then resuspended in either 10 mM or 1 μM (working solution for electrical detection) PBS buffer (pH 7.4), and allowed to rehydrate. Finally, SUVs were produced by point-probe sonication, yielding vesicles 50–100 nm in size. When vesicles were incubated on hydrophilic substrates above the transition temperature of the mixture, SLBs formed spontaneously via vesicle rupture and fusion. To image SLBs, DHPE-LR (Molecular Probes) fluorophores were mixed with phospholipids at 0.1% molar ratio. Polydimethyl siloxane³⁵ microfluidic channels with a typical cross-section of $10 \times 50 \mu\text{m}$ were laid on top of SWNT FETs to confine the liquid solution to the area proximal to the SWNTs (Fig. 1a). Images were obtained by using an upright Olympus fluorescence microscope with a thermo-electrically cooled 12-bit CCD camera (Cooke).

FCS MEASUREMENTS

FCS autocorrelation curves were acquired using a confocal fluorescence microscope in epi-illumination mode. Fluorescence was induced using a Coherent Sapphire laser (Model 488 – 02 CDRH) at 488 nm. The laser was passed through an excitation filter (Chroma Z488/ $\times 10$) and a $\times 10$ beam expander (Newport Corp) to completely fill the back aperture of the objective and achieve a diffraction limited illumination profile. Fluorescence was collected through a dichroic mirror (Chroma Z488RDC) and an emission filter (Chroma AF 535/45). A coverslip corrected $\times 60$, 1.2 NA water immersion objective was used on an Olympus IX71 microscope. Fluorescence was then coupled to an avalanche photodiode (SPCM-AQR-14-FC) by a 50- μm core fibre-optic patch cord. A flex02-12D correlator card (Correlator.com) was used to calculate FCS autocorrelation curves, and a PC was then used to acquire and record the intensity trace and correlation function. A power meter was used to monitor laser power and a set of neutral density filters (Chroma) was used to maintain an incident beam power of $\sim 100 \mu\text{W}$ to minimize photo-physical effects related to nonradiative states and photobleaching. The nanotube devices used for FCS measurements were fabricated on 170- μm -thick quartz wafers.

ELECTRICAL MEASUREMENTS

A 10-mV a.c. source–drain bias at 155 Hz was applied across the SWNT FETs and the conductance G was measured with a lock-in amplifier. A gold electrode immersed in the buffer solution controlled the potential V_c of the solution^{7,36}. All measurements were made in the same buffer after unfused vesicles and unbound proteins had been flushed out of the channel.

References

- McEuen, P. L. Single-wall carbon nanotubes. *Phys. World* **13**, 31–36 (June 2000).
- Kong, J. *et al.* Nanotube molecular wires as chemical sensors. *Science* **287**, 622–625 (2000).
- Star, A., Gabriel, J. C. P., Bradley, K. & Gruner, G. Electronic detection of specific protein binding using nanotube FET devices. *Nano Lett.* **3**, 459–463 (2003).
- Besteman, K., Lee, J. O., Wiertz, F. G. M., Heering, H. A. & Dekker, C. Enzyme-coated carbon nanotubes as single-molecule biosensors. *Nano Lett.* **3**, 727–730 (2003).
- Kong, J., Soh, H. T., Cassell, A. M., Quate, C. F. & Dai, H. J. Synthesis of individual single-walled carbon nanotubes on patterned silicon wafers. *Nature* **395**, 878–881 (1998).
- Zhou, X. J., Park, J. Y., Huang, S. M., Liu, J. & McEuen, P. L. Band structure, phonon scattering, and the performance limit of single-walled carbon nanotube transistors. *Phys. Rev. Lett.* **95**, 146805 (2005).
- Rosenblatt, S. *et al.* High performance electrolyte gated carbon nanotube transistors. *Nano Lett.* **2**, 869–872 (2002).
- Brian, A. A. & McConnell, H. M. Allogeneic stimulation of cytotoxic T cells by supported planar membranes. *Proc. Natl Acad. Sci. USA* **81**, 6159–6163 (1984).
- Sackmann, E. Supported membranes: scientific and practical applications. *Science* **271**, 43–48 (1996).
- Richard, C., Balavoine, F., Schultz, P., Ebbesen, T. W. & Mioskowski, C. Supramolecular self-assembly of lipid derivatives on carbon nanotubes. *Science* **300**, 775–778 (2003).
- Salafsky, J., Groves, J. T. & Boxer, S. G. Architecture and function of membrane proteins in planar supported bilayers: A study with photosynthetic reaction centers. *Biochemistry* **35**, 14773–14781 (1996).
- Mossman, K. D., Campi, G., Groves, J. T. & Dustin, M. L. Altered TCR signaling from geometrically repatterned immunological synapses. *Science* **310**, 1191–1193 (2005).
- Ye, J. S. *et al.* Self-assembly of bilayer lipid membrane at multivalued carbon nanotubes towards the development of photo-switched functional device. *Electrochem. Commun.* **7**, 81–86 (2005).
- Artyukhin, A. B. *et al.* Functional one-dimensional lipid bilayers on carbon nanotube templates. *J. Am. Chem. Soc.* **127**, 7538–7542 (2005).
- Bradley, K., Davis, A., Gabriel, J. C. P. & Gruner, G. Integration of cell membranes and nanotube transistors. *Nano Lett.* **5**, 841–845 (2005).
- Axelrod, D., Koppel, D. E., Schlessinger, J., Elson, E. & Webb, W. W. Mobility measurement by analysis of fluorescence photobleaching recovery kinetics. *Biophys. J.* **16**, 1055–1069 (1976).
- Magle, D., Elson, E. L. & Webb, W. W. Fluorescence correlation spectroscopy. II. Experimental realization. *Biopolymers* **13**, 29–61 (1974).
- Orth, R. N. *et al.* Creating biological membranes on the micron scale: Forming patterned lipid bilayers using a polymer lift-off technique. *Biophys. J.* **85**, 3066–3073 (2003).
- Groves, J. T., Ulman, N. & Boxer, S. G. Micropatterning fluid lipid bilayers on solid supports. *Science* **275**, 651–653 (1997).
- Ajo-Franklin, C. M., Yoshina-Ishii, C. & Boxer, S. G. Probing the structure of supported membranes and tethered oligonucleotides by fluorescence interference contrast microscopy. *Langmuir* **21**, 4976–4983 (2005).
- Stryer, L. Fluorescence energy transfer as a spectroscopic ruler. *Annu. Rev. Biochem.* **47**, 819–846 (1978).
- Parthasarathy, R., Yu, C. H. & Groves, J. T. Curvature-modulated phase separation in lipid bilayer membranes. *Langmuir* **22**, 5095–5099 (2006).
- Roux, A. *et al.* Role of curvature and phase transition in lipid sorting and fission of membrane tubules. *EMBO J.* **24**, 1537–1545 (2005).
- van Meer, G. & Vaz, W. L. Membrane curvature sorts lipids. Stabilized lipid rafts in membrane transport. *EMBO Rep.* **6**, 418–419 (2005).
- Moran-Mirabal, J. M. *et al.* Micrometer-sized supported lipid bilayer arrays for bacterial toxin binding studies through total internal reflection fluorescence microscopy. *Biophys. J.* **89**, 296–305 (2005).
- Angstrom, J., Teneberg, S. & Karlsson, K. A. Delineation and comparison of ganglioside-binding epitopes for the toxins of *Vibrio cholerae*, *Escherichia coli*, and *Clostridium tetani*: evidence for overlapping epitopes. *Proc. Natl Acad. Sci. USA* **91**, 11859–11863 (1994).
- Graneli, A., Yeykal, C. C., Robertson, R. B. & Greene, E. C. Long-distance lateral diffusion of human Rad51 on double-stranded DNA. *Proc. Natl Acad. Sci. USA* **103**, 1221–1226 (2006).
- Pesen, D. & Hoh, J. H. Micromechanical architecture of the endothelial cell cortex. *Biophys. J.* **88**, 670–679 (2005).
- Bonetta, L. Spectrin is peripheral. *J. Cell. Biol.* **170**, 12 (2005).
- Tank, D. W., Wu, E. S. & Webb, W. W. Enhanced molecular diffusibility in muscle membrane blebs: release of lateral constraints. *J. Cell. Biol.* **92**, 207–212 (1982).
- Kusumi, A., Ike, H., Nakada, C., Murase, K. & Fujiwara, T. Single-molecule tracking of membrane molecules: plasma membrane compartmentalization and dynamic assembly of raft-philic signaling molecules. *Semin. Immunol.* **17**, 3–21 (2005).
- Chalet, L. & Wolf, F. J. Properties of streptavidin biotin-binding protein produced by streptomycetes. *Arch. Biochem. Biophys.* **106**, 1–5 (1964).
- Artyukhin, A. B. *et al.* Controlled electrostatic gating of carbon nanotube FET devices. *Nano Lett.* **6**, 2080–2085 (2006).
- Groves, J. T., Wulfing, C. & Boxer, S. G. Electrical manipulation of glycan-phosphatidyl inositol-tethered proteins in planar supported bilayers. *Biophys. J.* **71**, 2716–2723 (1996).
- Ng, J. M. K., Gitlin, I., Stroock, A. D. & Whitesides, G. M. Components for integrated poly(dimethylsiloxane) microfluidic systems. *Electrophoresis* **23**, 3461–3473 (2002).
- Larrimore, L., Nad, S., Zhou, X. J., Abruna, H. & McEuen, P. L. Probing electrostatic potentials in solution with carbon nanotube transistors. *Nano Lett.* **6**, 1329–1333 (2006).

Acknowledgements

This work was supported by the Nanobiotechnology Center (NBTC), an STC Program of the National Science Foundation under Agreement No. ECS-9876771. J.M.M. thanks CONACyT for support through its graduate fellowship programme. Sample fabrication was performed at the Cornell Nanoscale Science & Technology Facility, a member of the National Nanotechnology Infrastructure Network, which is supported by the National Science Foundation (Grant ECS 03-35765). Supplementary information accompanies this paper on www.nature.com/naturenanotechnology. Correspondence and requests for materials should be addressed to X.Z. or P.L.M.

Author contributions

X.Z. and J.M. performed the experiments and analysed the data. All the authors discussed the results and co-wrote the manuscript.

Competing financial interests

The authors declare that they have no competing financial interests.

Reprints and permission information is available online at <http://npg.nature.com/reprintsandpermissions/>